

1 Sea ice algae as victims of their own success

2 Anthony R. Jajeh, Kenneth M. Golden, Jody W. Deming, Jody R. Reimer

3 January 28, 2026

4 **Abstract** Algae living in the brine inclusions of polar sea ice produce a protective gelatinous coating of
5 extracellular polymeric substances (EPS), which helps them survive in their harsh sea-ice habitat. One con-
6 sequence of EPS production may be a reduction in nutrient availability, as EPS alters the ice microstructure,
7 reducing permeability and the flux of nutrient-rich seawater into the ice. Here, we identify and analyze a
8 novel biophysical feedback loop in which algae modify their environment through EPS production, which
9 then affects nutrient availability and subsequent algal growth. While mathematical models coupling nutri-
10 ent and algal dynamics have been widely used to understand bloom dynamics, we here introduce EPS as an
11 additional variable to facilitate the investigation of this feedback. Analysis of both transient and asymptotic
12 dynamics suggests that EPS-mediated feedbacks suppress algal biomass in both the short and long term.
13 Quasi-steady-state analysis of our model reveals a transcritical bifurcation governed by nutrient fluxes, in-
14 dicating a threshold beyond which the system transitions from a barren state to one supporting microbial
15 life. We also identify a Hopf bifurcation, which suggests that EPS-mediated negative feedbacks can give rise
16 to sustained oscillations in nutrient and algal biomass levels. These results highlight how the tight coupling
17 between EPS production, nutrient transport, and algal dynamics fundamentally shapes both sea ice primary
18 productivity and permeability.

19 1 Introduction

20 Polar sea ice hosts a dynamic community of microscopic inhabitants within its porous microstructure [3].
21 This microstructure forms as seawater freezes, concentrating the salt into brines. Much of the brine is ex-
22 pelled, but some remains trapped within the ice, creating a network of brine-filled inclusions [16, 20, 30].
23 Ice algae dominate these brine inclusions in spring, when light becomes sufficient to support algal blooms
24 in the ice [25]. Ice algae contribute significantly (up to 26% [8]) to total primary production in the Polar Re-
25 gions [1]. Due to their early availability in spring and lipid-rich composition [8], ice algae are foundational
26 to the polar marine food web, supporting grazers such as zooplankton, which in turn support higher trophic
27 levels, including fish, seabirds, whales, seals, and polar bears [25].

28 Ice algae must endure extreme environmental conditions within the ice, including low temperatures, high
29 salinity, and low light availability for much of the year. Many sea-ice microbes, including ice algae, have
30 adapted by producing a cryoprotective gelatinous coating of extracellular polymeric substances (EPS), a
31 complex mix of polysaccharides, proteins, and other components [5, 15]. In addition to acting as a buffer
32 between the microbes and their environment, EPS alters the physical properties of the surrounding ice [15,
33 22]. As it accumulates in the ice, EPS changes the geometry of the pores and may impede fluid flow through
34 clogging effects, altering the flux of nutrients available to the microbial community [15, 24]. Reduced

35 nutrient fluxes (in particular, nitrogen, silica, and carbon) limit algal growth [8], and because algae are the
36 largest producers of EPS, this is hypothesized to subsequently decrease EPS production rates. This suggests
37 a complex EPS-mediated biophysical feedback, with implications for both sea ice physics and ecosystem
38 dynamics.

39 In this paper, we take the first step toward understanding the biophysical feedback dynamics mediated
40 by EPS. We begin with a canonical algal bloom model and extend it to include EPS dynamics (Section
41 2). This model is a coupled set of ordinary differential equations that describes the interactions among
42 nutrients, algae, and EPS. While we do not explicitly model sea ice microstructure, the effect of EPS on ice
43 permeability is included through nonlinear terms that capture its impact on nutrient fluxes. In Section 2.1,
44 we analyze the most general form of the model to understand its key features of asymptotic behavior. In
45 Section 2.2, we explore model sensitivity to the timescales over which EPS accumulates and decays, as these
46 processes are difficult to measure empirically and thus poorly constrained in our model. We analyze three
47 model regimes corresponding to three timescale assumptions: EPS dynamics are much slower than algal and
48 nutrient dynamics (Regime 1, Section 2.2.1); EPS dynamics are fast, responding instantaneously to changes
49 in algal biomass (Regime 2, Section 2.2.2); and EPS dynamics occur over similar timescales to those of
50 algae and nutrients (Regime 3, Section 2.2.3). We conduct a bifurcation and stability analysis of our model
51 under each of these assumptions. Comparison between regimes (Section 2.3) reveals a persistent transcritical
52 bifurcation that depends on nutrient flux terms, and a Hopf bifurcation that is only possible if EPS dynamics
53 occur over similar timescales to those of algae and nutrients (Regime 3). This Hopf bifurcation suggests that
54 strong EPS-mediated negative feedbacks may induce periodic algal growth and, fascinatingly, concurrent
55 periodic changes in ice permeability. Finally, in Section 2.4, we investigate the system’s transient bloom
56 dynamics through numerical simulations. The transient dynamics show that the inverse relationship between
57 EPS accumulation and peak bloom intensity suggests that the negative EPS-mediated biophysical feedbacks
58 that are the focus of this paper reduce peak algal concentrations.

59 **2 Model formulation**

60 We begin with a classic model of nutrient-driven phytoplankton blooms [11], which captures the main
61 processes and functional forms commonly found in sea ice biogeochemical models [17, 19, 22, 26].

$$\begin{aligned}\frac{dN}{dt} &= \alpha - \frac{\nu N A}{\gamma + N} - \beta N \\ \frac{dA}{dt} &= \xi \frac{\nu N A}{\gamma + N} - \delta A\end{aligned}$$

62 Typically, this model describes the dynamics of a limiting nutrient N and phytoplankton P ; however, since
63 algae are our primary producers of interest, we have changed the notation from P to A . We have chosen
64 nitrogen as the nutrient of interest, as nitrogen limitation is hypothesized to inhibit ice algal blooms[12].
65 Nutrient fluxes are described as input (α) and loss (β) rates, assuming nutrients enter the brine inclusions
66 from the ocean below, facilitated by convective processes within the ice [20]. Nutrient uptake by algae
67 is described by the Monod term in both equations, where ν is the maximum uptake rate, γ is the half-
68 saturation constant, and ξ is the rate of algal growth corresponding to nutrient uptake. Algae are lost at a
69 rate δ due to death or loss from the ice. All parameter values are assumed to be positive. Note that this model
70 assumes constant, optimal light for photosynthesis. and an unchanging ice environment corresponding to
71 stable temperatures.

72 We now adapt this model to study EPS-mediated biophysical feedbacks. We add E , a state variable de-
 73 scribing the concentration of EPS in the system. We assume EPS accumulation is proportional (ρ) to the
 74 amount of algae present, and that it decays at a constant rate (η). As EPS accumulates, it clogs the brine
 75 inclusions, reducing nutrient fluxes [15]. To capture this process, we replace the parameters α and β in the
 76 above equations with EPS-dependent functions, $\alpha(E)$ and $\beta(E)$. The resulting model of coupled nutrient,
 77 algae, and EPS dynamics is

$$\begin{aligned}\frac{dN}{dt} &= \alpha(E) - \frac{\nu NA}{\gamma + N} - \beta(E)N \\ \frac{dA}{dt} &= \xi \frac{\nu NA}{\gamma + N} - \delta A \\ \frac{dE}{dt} &= \rho A - \eta E\end{aligned}\tag{1}$$

78 Table 1 describes the units of each model component and the values of model parameters, where available,
 79 from the literature.

Symbol	Biological Description	Value	Range	Units	Source
N	Average concentration of particulate nitrogen	N/A	0.1–0.2	mg N/L	[15] Supp. Table S2
A	Mean chl a in bottom 10 cm of sea ice	N/A	0.03–0.06	mg/L	[15] Supp. Table S2
E	EPS concentration	N/A	0.8–7.7	mg XG/L	[14]
N_0	Initial condition of nutrients	0.2	-	mg N/L	Prescribed
A_0	Initial condition of algae	0.0002	-	mg A/L	Prescribed
E_0	Initial condition of EPS	0.002	-	mg XG/L	Prescribed
ϕ	Inflow of nutrients	0.01	-	mg N/(L day)	Prescribed
ψ	Outflow rate of nutrients	0.01	-	1/day	Prescribed
ν	Uptake rate of bottom ice algae	0.2	0.24	mg N/(mg chl a day)	[12]
ρ	Production rate of EPS	.75	0.1–1	mg XG/(mg chl a L day)	[14]
δ	Mortality rate of diatoms	0.007	0.007	1/day	[9]
η	Bacterial degradation of polysaccharides	0.03	0.03	1/day	[9]
γ	Nitrogen half-saturation constant of diatoms	0.01	0.01	mg N/L	[9]
ξ	Algal chla to nitrogen conversion ratio	0.2	0.2	mg chl a/mg N	[9]
μ	Strength of EPS feedback	0.001	-	mg XG/L	Prescribed
σ	Scaling of how EPS tracks algae in Regime 2	0.05	-	-	Prescribed

Table 1: State variables and parameter values used throughout this work. Rows for the state variables N , A , and E describe their observed average concentrations in spring sea ice for comparison with our model outputs. The Value column contains the parameter values chosen as the defaults for all figures produced in the text unless noted otherwise. The Range column contains the parameter ranges documented in the literature described under Source.

80 **2.1 A nutrient-driven transcritical bifurcation**

81 Empirical estimates of the best form for the nutrient flux functions, $\alpha(E)$ and $\beta(E)$, do not exist, so we
 82 first analyze model (1) without explicitly specifying functional forms, assuming only that they are positive.
 83 Setting $\frac{dN}{dt} = \frac{dA}{dt} = \frac{dE}{dt} = 0$, we find two steady-state solutions for (N^*, A^*, E^*) :

$$s_0 := \left(\frac{\alpha(0)}{\beta(0)}, 0, 0 \right)$$

$$s_1 := \left(\frac{-\delta\gamma}{-\xi\nu + \delta}, \frac{\xi\beta(E)}{\delta(\delta - \xi\nu)} \left(\gamma\delta + \frac{\alpha(E)}{\beta(E)}(\delta - \xi - \nu) \right), \frac{\rho A^*}{\eta} \right)$$

84 Observe that s_0 is a trivial steady state, characterized by the absence of both algae and EPS, while s_1 is a
 85 nontrivial steady state in which algae and EPS persist. To assess the stability of s_0 , we analyze the Jacobian
 86 of (1) evaluated at this steady state (see S1), which yields the following eigenvalues:

$$\lambda_1 = -\eta, \quad \lambda_2 = -\beta(0), \quad \lambda_3 = \frac{\xi\nu\alpha(0) - \beta(0)\gamma\delta - \alpha(0)\delta}{\gamma\beta(0) + \alpha(0)}$$

87 Because all model parameters and α and β are positive, λ_1 and λ_2 are negative, and the sign of λ_3 depends
 88 on the sign of its numerator. Rearranging, we see that if $\alpha(0)/\beta(0) < \gamma\delta/(\xi\nu - \delta)$, then $\lambda_3 < 0$ and s_0 is a
 89 stable node. So if the ratio of nutrient input to loss in the absence of EPS, $\alpha(0)/\beta(0)$, is sufficiently small,
 90 the system will eventually approach an algae- and EPS-free state. However, if $\alpha(0)/\beta(0)$ is sufficiently
 91 large, then $\lambda_3 > 0$ and s_0 is unstable. This is a transcritical bifurcation in the ratio of nutrient input to loss
 92 in an EPS-free system, $\alpha(0)/\beta(0)$. This behavior provides a key ecological insight: algae persist only when
 93 nutrient inflow is sufficiently large relative to nutrient outflow, replenishing the nutrients needed to sustain
 94 the algal population. We will see this reflected in several places in the analysis that follows.

95 The nontrivial equilibrium s_1 is only defined if all state variables are nonnegative, that is, if $\frac{\alpha(E)}{\beta(E)} \geq \frac{\gamma\delta}{\nu\xi - \delta}$,
 96 with $\delta < \xi\nu$. We cannot further analyze the existence and stability of s_1 without specifying functional forms
 97 for $\alpha(E)$ and $\beta(E)$. We here choose to use a negative exponential function, which captures the hypothesis
 98 that higher EPS reduces nutrient fluxes. We define $\alpha(E) = \phi \exp(-\frac{E}{\mu})$ and $\beta(E) = \psi \exp(-\frac{E}{\mu})$, where ϕ
 99 and ψ represent the nutrient input and loss rates in the absence of EPS, respectively, and μ is the strength of
 100 EPS limitation. This results in the fully specified model

$$\begin{aligned} \frac{dN}{dt} &= \phi e^{-\frac{E}{\mu}} - \frac{\nu N}{\gamma + N} A - \psi e^{-\frac{E}{\mu}} N \\ \frac{dA}{dt} &= \xi \frac{\nu A N}{\gamma + N} - \delta A \\ \frac{dE}{dt} &= \rho A - \eta E \end{aligned} \tag{2}$$

101 **2.2 Model analysis under different timescale assumptions**

102 It is difficult to measure EPS within sea ice, and the methods that do exist require melting the ice to extract
 103 the EPS, making in situ serial measurements impossible [19]. Because of this, little is known about how
 104 rapidly EPS accumulates or decays within sea ice. We explore three possible temporal regimes by modifying
 105 and analyzing (2) accordingly.

106 **2.2.1 Regime 1: EPS dynamics are much slower than algae and nutrient dynamics**

107 We start by nondimensionalizing (2) (see Appendix C) with this temporal scaling in mind. This results in
108 two fast equations and one slow one,

$$\text{Fast} \begin{cases} \epsilon \frac{dN}{d\tau} = ae^{-E} - \frac{cAN}{N+1} - bNe^{-E} \\ \epsilon \frac{dA}{d\tau} = \frac{fNA}{N+1} - A \end{cases} \quad (3a)$$

$$\text{Slow} \begin{cases} \frac{dE}{d\tau} = dA - E \end{cases} \quad (3b)$$

109 We now perform a quasi-steady-state analysis of our system. To analyze the fast set of equations, we scale
110 time by ϵ , that is, $\tau' = \frac{\tau}{\epsilon}$. Then (3) becomes:

$$\frac{dN}{d\tau'} = ae^{-E} - \frac{cAN}{N+1} - bNe^{-E} \quad (4a)$$

$$\frac{dA}{d\tau'} = \frac{fNA}{N+1} - A \quad (4b)$$

$$\frac{dE}{d\tau'} = \epsilon(dA - E) \quad (4c)$$

111 We now let $\epsilon \rightarrow 0$. In the dimensional model, this is equivalent to $\epsilon = \eta/\delta \rightarrow 0$, which corresponds to the
112 assumption that algal loss occurs at a much faster rate than EPS decay ($\delta \gg \eta$). In this limit, EPS remains
113 at its initial value, $E(t) = E(0) = E_0$. We now analyze the remaining two equations, (4a) and (4b). Setting
114 $\frac{dN}{d\tau'} = \frac{dA}{d\tau'} = 0$, we find two steady-state solutions:

$$p_0 := \left(\frac{a}{b}, 0 \right)$$

$$p_1 := \left(\frac{1}{f-1}, \frac{f(af-a-b)}{e^{E_0}c(f-1)} \right).$$

115 Again, we find a trivial, algae-free solution p_0 , as well as a possible nontrivial solution p_1 with persistent
116 algae, provided $\frac{a}{b} > \frac{1}{(f-1)} > 0$, which is necessary to guarantee positive entries in p_1 . Evaluating the
117 Jacobian of the matrix differential of (4a)-(4b) at p_0 yields the following eigenvalues see S2):

$$\lambda_1 = -be^{-E_0}, \lambda_2 = \frac{af-a-b}{a+b}$$

118 Since λ_1 will always be negative, the stability of p_0 is determined by the sign of λ_2 . The sign of λ_2 hinges
119 on the same inequality as the existence of p_1 , specifically the relationship between $\frac{a}{b}$ and $\frac{1}{(f-1)}$. If p_1 exists,
120 then p_0 is unstable, since $\frac{a}{b} > \frac{1}{(f-1)}$ and so $\lambda_2 > 0$. If p_1 does not exist, p_0 is stable, since $\frac{a}{b} < \frac{1}{(f-1)}$ and
121 so $\lambda_2 < 0$ (Figure 1).

122 Turning our attention to the stability of the nontrivial equilibrium, we evaluate the Jacobian at p_1 (see S2):

$$J_{p_1} = \begin{bmatrix} -\frac{e^{-E_0}(f^2a-2af+a+b)}{c} & -\frac{c}{f} \\ \frac{(af-a-b)e^{-E_0}(f-1)}{c} & 0 \end{bmatrix}$$

123 We use the trace and determinant to determine stability. If $\frac{a}{b} > \frac{1}{(f-1)}$, then the trace of the Jacobian is
124 negative and the determinant is positive, confirming that p_1 becomes a stable sink for the same values of $\frac{a}{b}$
125 at which p_0 loses stability (Figure 1). This result echoes our findings in Section 2.1, where we identified a
126 transcritical bifurcation governed by the balance between nutrient inflow and outflow.

127 We also rule out the possibility of a Hopf bifurcation for this system. For a Hopf bifurcation, the trace of
 128 the Jacobian would need to be zero:

$$\text{Trace}(J_{p_1}) = 0 \implies f^2a - 2af + a + b = 0 \implies \frac{a}{b} = \frac{-1}{(f-1)^2}$$

129 which is not possible for nonnegative values of a and b .

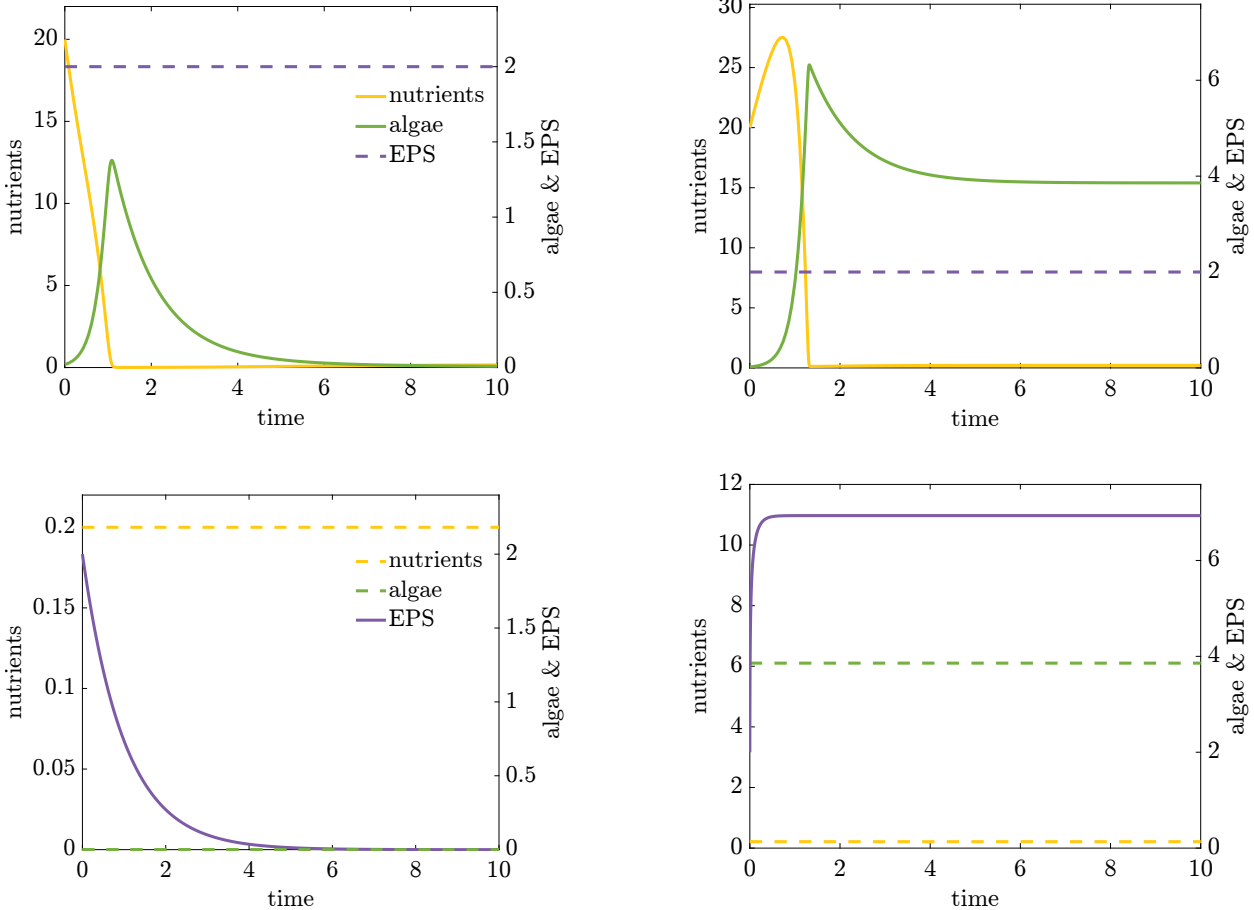


Figure 1: Two possible asymptotic dynamics arise under Regime 1, where we assume EPS dynamics are much slower than algae and nutrient dynamics. **Top row:** nutrients and algae evolve on the fast timescale while EPS is held fixed at its quasi-steady state value, ($E = E_0$). **Bottom row:** nutrients and algae are assumed to instantaneously reach their fast quasi-steady state p_0 and p_1 , respectively, reducing the system to a single slow EPS equation. **Left column:** Parameters are such that nutrient loss exceeds nutrient input, resulting in algae and EPS asymptotically approaching 0. Dimensional parameters are as in Table 1, except for $\phi = .0001$ and $\psi = .05$. Corresponding nondimensional parameters are $a = 1.4, b = 7.1, f = 5.7$ thus $\frac{a}{b} < \frac{1}{f-1}$. **Right column:** Nutrient input is sufficient to sustain algae and EPS asymptotically. Parameters are as in Table 1, here nondimensional parameters $a = 142.9, b = 1.4, f = 5.7$ thus $\frac{a}{b} > \frac{1}{f-1}$.

130 We now focus on the slow model dynamics of (3b). For this analysis, we do not rescale time, so when we let
 131 $\epsilon \rightarrow 0$, the left-hand side of the equations in (3a) becomes zero. In this quasi-steady-state limit, we find the
 132 same two nutrient and algae equilibria as in the fast system above, p_0 and p_1 . In the trivial quasi-steady state
 133 p_0 , (3b) simplifies to $\frac{dE}{d\tau} = -E$, so EPS decays exponentially from its initial condition $E(0)$ in the absence
 134 of algae. This behavior is biologically reasonable, as no new EPS is produced in the absence of algae, and

135 any existing EPS decays. If we instead substitute the nontrivial quasi-steady state p_1 into (3b), we have

$$\frac{dE}{d\tau} = \frac{fd(af - a - b)}{e^E c(f - 1)} - E. \quad (5)$$

136 This results in a nontrivial steady-state solution for EPS (Figure 1),

$$E^* = W\left(\frac{fd(af - a - b)}{c(f - 1)}\right)$$

137 where $W(\cdot)$ is the Lambert W function. The Lambert W function is defined as the solution $W(x)$ to the
 138 transcendental equation $We^W = x$ with real domain $x \in [-\frac{1}{e}, \infty)$. Note that in order for $W(\cdot) > 0$ and
 139 an equilibrium point E^* to exist, the argument of the Lambert W function is nonnegative, which requires
 140 $af - a - b \geq 0$, or equivalently $\frac{a}{b} > \frac{1}{f-1}$. To assess the local stability of E^* , we differentiate the right-hand
 141 side of equation (5) with respect to E and evaluate at E^* , which yields:

$$\frac{d}{dE} \left(\frac{dE}{d\tau} \right) \Big|_{E=E^*} = -W\left(\frac{fd(af - a - b)}{c(f - 1)}\right) - 1 \quad (6)$$

142 The stability of E^* is determined by the sign of (6), which depends on $W\left(\frac{fd(af - a - b)}{c(f - 1)}\right)$. Since $W(-\frac{1}{e}) =$
 143 -1 , a change in stability occurs when

$$\frac{fd(af - a - b)}{c(f - 1)} = -\frac{1}{e}. \quad (7)$$

144 We can reframe this relationship in terms of the ratio of nutrient fluxes, $\frac{a}{b}$,

$$\frac{a}{b} = \frac{-c}{efdb} + \frac{1}{f-1}$$

145 When $\frac{a}{b}$ is greater than this threshold, then E^* in the slow model is stable (Figure 1).

146 In the fast model, algae persist when $\frac{a}{b} > \frac{1}{(f-1)}$. Because (5) assumes the same nontrivial algal steady state
 147 as in the fast model, if

$$\frac{a}{b} > \frac{1}{f-1} > \frac{-c}{efbd} + \frac{1}{f-1},$$

148 then, algae in the fast model will rapidly reach a nontrivial steady state, with a corresponding nontrivial
 149 EPS steady state in the slow model. This fast-slow analysis reveals dynamics consistent with our previous
 150 findings: if nutrient input rates are sufficiently high relative to nutrient loss, the system can sustain positive
 151 algae and EPS concentrations asymptotically.

152 2.2.2 Regime 2: EPS dynamics are fast, responding instantaneously to changes in algal biomass

153 In the previous section, we considered a possible regime where EPS dynamics are much slower than those
 154 of nutrients and algae. Here, we consider the implications of the opposite extreme: EPS responds instanta-
 155 neously to changes in nutrient and algae levels. Mathematically, we model this by assuming EPS perfectly
 156 tracks algae, so $E(t) = \sigma A(t)$, where σ is a scaling term. Under this assumption, model (2) becomes

$$\begin{aligned} \frac{dN}{dt} &= \phi e^{-\frac{\sigma A}{\mu}} - \frac{\nu N}{\gamma + N} A - \psi e^{-\frac{\sigma A}{\mu}} N \\ \frac{dA}{dt} &= \xi \frac{\nu AN}{\gamma + N} - \delta A \\ E(t) &= \sigma A(t). \end{aligned} \quad (8)$$

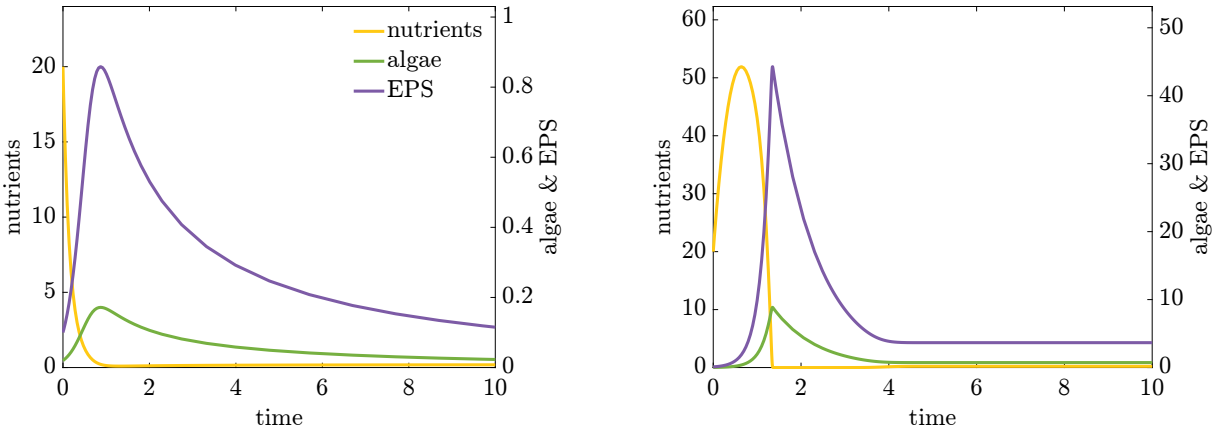


Figure 2: Two possible asymptotic regimes under Regime 2, arising from timescale separation in which EPS dynamics track algal dynamics. In this regime, EPS adjusts on the same fast timescale as algae and nutrient dynamics. **Left to right:** parameter values transition from a regime in which nutrient loss exceeds nutrient input ($\frac{a}{b} < \frac{1}{f-1}$), resulting in algal extinction and stability of the trivial equilibrium p_0 , to a regime in which nutrient input dominates loss ($\frac{a}{b} > \frac{1}{f-1}$), yielding a stable positive algal equilibrium p_1 . **Left:** Dimensional parameters are as in Table 1, except for $\phi = .0001$ and $\psi = .05$. for the left column. Here, nondimensional parameters are $a = 1.4, b = 7.1, f = 5.7$ thus $\frac{a}{b} < \frac{1}{f-1}$. **Right:** Parameters are as in Table 1, here, nondimensional parameters $a = 142.9, b = 1.4, f = 5.7$ thus $\frac{a}{b} > \frac{1}{f-1}$.

157 Nondimensionalizing the system (Appendix D) yields:

$$\begin{aligned} \frac{dN}{dt} &= ae^{-hA} - \frac{cNA}{N+1} - bNe^{-hA} \\ \frac{dA}{dt} &= \frac{fNA}{N+1} - A \\ E(t) &= hA \end{aligned} \tag{9}$$

158 We ignore $E(t)$ in our analysis, since $E(t)$ dynamics are directly proportional to $A(t)$. This system again
159 has two steady-state solutions for N and A :

$$\begin{aligned} r_0 &= \left(\frac{a}{b}, 0 \right) \\ r_1 &= \left(\frac{1}{f-1}, \frac{W\left(hf\frac{(af-a-b)}{c(f-1)}\right)}{h} \right), \end{aligned}$$

160 corresponding to a trivial, algal-free steady state r_0 , and a nontrivial steady state r_1 with persistent algae
161 (and thus persistent EPS at concentration $E^* = hA^*$).

162 Evaluating the Jacobian of the matrix differential equation of (9) at r_0 yields the following eigenvalues (see
163 S3):

$$\lambda_1 = -b, \quad \lambda_2 = \frac{af - a - b}{a + b}.$$

164 λ_1 is always negative, so the stability of r_0 is determined by the sign of λ_2 . As in Section 2.2.1, we find that
165 r_0 loses stability through a transcritical bifurcation at $\frac{a}{b} = \frac{1}{(f-1)}$, demonstrating the importance of nutrient
166 fluxes in sustaining persistent algal communities.

167 Observe that this transcritical bifurcation occurs exactly at the point where the entries of r_1 become non-
168 negative.

169 Due to the presence of the Lambert W function, analyzing the stability of r_1 is not as straightforward as
170 evaluating the Jacobian of (9) at r_1 . Instead, we proceed as follows. First, we substitute $N^* = \frac{1}{f-1}$ into (9)
171 to obtain an expression for A^* as a function of system parameters:

$$\frac{dN}{dt} = ae^{-hA^*} - \frac{cA^*}{f} - \frac{be^{-hA^*}}{f-1} = 0.$$

172 We can then rearrange this expression in terms of one of our parameters, here chosen to be b ,

$$b = (f-1)(a - cA^*e^{hA^*}/f). \quad (10)$$

173 Plugging this expression into both $\frac{dN}{dt}$ and $\frac{dA}{dt}$ in (9), we can evaluate the Jacobian of (9), finding the
174 determinant and trace as functions of A^* (see S3):

$$Det(J_{r_1}) = \frac{(hA^* + 1) cA^* (f - 1)^2}{f^2} \quad (11)$$

$$Tr(J_{r_1}) = \frac{(f - 1) \left(-e^{-hA^*} a f^2 + cA^* \right)}{f^2} \quad (12)$$

175 The determinant is always nonnegative, and it can be proven that the trace is always negative (Appendix B),
176 so this equilibrium is stable.

Next, we ask whether a Hopf bifurcation could occur by examining the condition $Tr(J_{r_1}) = 0$. Setting the trace to zero in (12) gives:

$$cA^* = af^2e^{-ha}$$

177 Substituting this term into the expression for b in equation (10), we compute:

$$\begin{aligned} sign(b) &= sign(-cA^* + afe^{-hA^*}) \\ &= sign(-af^2e^{-hA^*} + afe^{-hA^*}) \\ &= sign(-afe^{-hA^*}(f + 1)) \\ &< 0 \end{aligned}$$

178 Again, we see that achieving $Tr(J_{r_1}) = 0$ requires $b < 0$, which is biologically implausible. Hence, for all
179 positive parameter values, $Tr(J_{r_1}) < 0$, and the equilibrium point r_1 is a stable sink (Figure 2).

180 2.2.3 Regime 3: EPS dynamics occur over similar timescales to those of algae and nutrients

181 The final regime explores the hypothesis that EPS dynamics occur on a timescale similar to that of algae and
182 nutrients, requiring us to consider the full system of three ODEs in (2). We have already nondimensionalized
183 this model in (3), and we now analyze the full system dynamics rather than making a quasi-steady-state
184 assumption, as was done in Section 2.1. The steady states (N^*, A^*, E^*) of (3) are:

$$\begin{aligned} q_0 &= \left(\frac{a}{b}, 0, 0 \right) \\ q_1 &= \left(\frac{1}{f-1}, \frac{1}{d} W \left(\frac{(af - a - b)fd}{c(f-1)} \right), W \left(\frac{(af - a - b)fd}{c(f-1)} \right) \right) \end{aligned}$$

185 Notice the similarity to the equilibria p_0 and p_1 in Regime 1 (Section 2.2.1) and r_0 and r_1 in Regime 2
186 (Section 2.2.2). As in Section 2.2.2, the nontrivial EPS steady state is a scalar multiple of the algal steady

187 state. Note that N^* in q_1 is only plausible if $f \geq 1$. As above in Regime 1 (Section 2.2.1), this transcritical
188 bifurcation occurs exactly at the point where the Lambert W entries of q_1 become nonnegative.

To determine the stability of q_0 , we examine the eigenvalues of the Jacobian of (3) at q_0 , (see S4):

$$\lambda_1 = -1, \lambda_2 = -b, \lambda_3 = \frac{af - a - b}{a + b}.$$

189 As in the previous two regimes, the trivial steady state q_0 is stable if $\frac{a}{b} < \frac{1}{f-1}$, and it is the ratio of nutrient
190 input to loss that determines algal persistence (Figure 3).

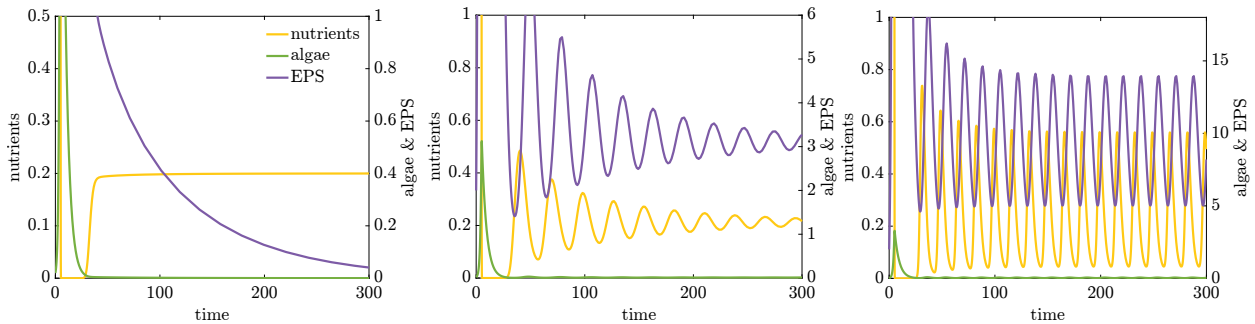


Figure 3: Three possible asymptotic regimes under Regime 3, arising from the ratio of inflow of nutrients to outflow of nutrients as seen in 4. **Left:** When the ratio of nutrient input to loss is too low ($\frac{a}{b} < \frac{1}{f-1}$), then the system is asymptotically free from algae and EPS (q_0 is stable). Parameters are as in Table 1, except $\phi = .0001$ and $\psi = .05$ which corresponds to nondimensional parameters $a = 1.4, b = 71.4, f = 5.7$. **Middle:** As $\frac{a}{b}$ increases and crosses the transcritical bifurcation threshold, we get a stable spiral towards the nontrivial equilibrium, q_1 . Parameters are as in Table 1, except $\phi = .0001$ and $\psi = .001$ with nondimensional parameters $a = 1.4, b = .14, f = 5.7$. **Right:** When (a, b) is on the right side of the manifold (Figure 4), we get a limit cycle around equilibrium point q_1 . Here, parameters are as in Table 1.

191 We next examine the stability of q_1 , where algae and EPS persist. Numerical bifurcation diagrams suggest
192 that immediately following the transcritical bifurcation, the nontrivial steady state q_1 is a stable spiral, and
193 that increasing nutrient input far enough leads not only to persistent algae and EPS but may eventually
194 result in periodic dynamics through a Hopf bifurcation (Figure 3). Motivated by these numerical findings,
195 we look for two bifurcations: one where the eigenvalues of the Jacobian evaluated at the nontrivial fixed
196 point become negative, signifying the stability of q_1 ; and one where a complex conjugate pair of eigenvalues
197 becomes purely imaginary, signifying periodic asymptotic dynamics.

198 In sections 2.2.1 and 2.2.2, the system was two-dimensional, allowing stability to be determined from the
199 trace and determinant of the Jacobian. In the full three-dimensional model, this approach is no longer suf-
200 ficient. Moreover, q_1 involves the Lambert W function, which makes direct substitution into the Jacobian
201 algebraically cumbersome. For this reason, we instead work symbolically with the Jacobian and impose
202 steady-state relationships later in the calculation, thereby avoiding explicit Lambert W terms.

203 To explore the possibility of a periodic solution, we construct the full Jacobian J_{q_1} , evaluate it at the
204 fixed point q_1 (see S4), and analyze its eigenvalues. We construct a modified characteristic polynomial,
205 $p_{char} = \det(J_{q_1} - i\sqrt{\omega}I)$, where $i\sqrt{\omega}$ are the purely complex eigenvalues of the system. The roots of the
206 characteristic polynomial may contain both real and imaginary parts. At a Hopf bifurcation, we require both
207 parts to vanish simultaneously. Therefore, we set $R = \text{Re}(p_{char}) = 0$ and $\text{Im}(p_{char}) = 0$. We first solve

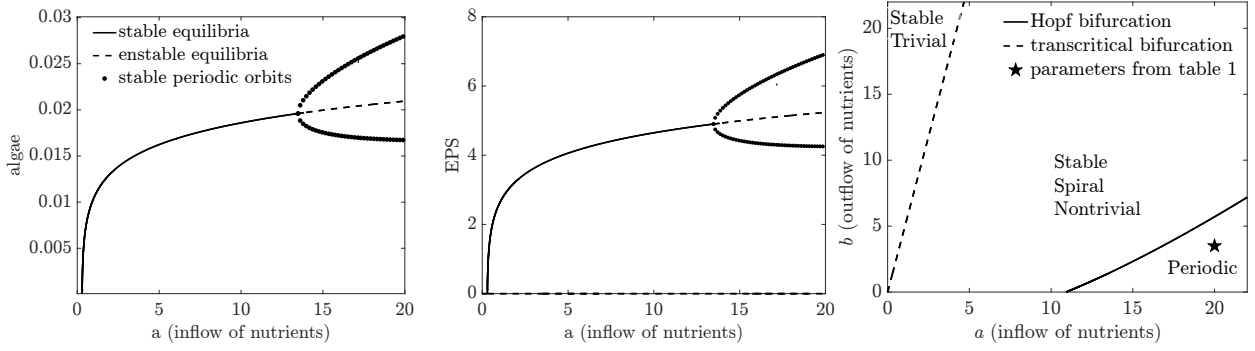


Figure 4: Bifurcation diagrams for regime 3. **Left:** Bifurcation diagram of asymptotic algal biomass, A . **Middle:** Bifurcation diagram of asymptotic EPS biomass, E . **Right:** Bifurcation diagram of both inflow of nutrients, a , and outflow of nutrients, b . For values of a slightly larger than 0, a transcritical bifurcation occurs in which the trivial equilibrium loses stability and a stable nonzero equilibrium emerges. As a increases further, the nontrivial equilibrium undergoes a Hopf bifurcation, giving rise to stable periodic oscillations. Parameters are as in Table 1.

208 $Im(p_{char}) = 0$, which gives an expression for ω (see S4). Next, we consider $Re(p_{char}) = 0$, but solving
 209 this equation directly for ω is challenging because the state variables N , A , and E appear in the expression.
 210 To address this challenge, we impose the steady-state conditions from the nondimensional system (3), so

$$E^* = dA^*$$

211 and

$$N^* = \frac{1}{f-1}.$$

212 Substituting these terms into the differential equation for $\frac{dN}{dt}$ yields an expression that depends on several
 213 parameters and the state variable A :

$$\frac{dN}{dt} = \frac{f(af - a - b)e^{-dA^*} - cA^*(f-1)}{f(f-1)}$$

214 Setting $\frac{dN}{dt} = 0$ gives the steady state relationship between parameters and A ,

$$b = -\frac{(f-1)(cA^*e^{dA^*} - af)}{f}.$$

215 Now, With both ω and b expressed analytically (See S4), we can find the solutions to $Re(p_{char}) = 0$.
 216 We choose to express these solutions in terms of a , maintaining our interest in how nutrient fluxes shape
 217 system dynamics. a appears quadratically in $Re(p_{char})$, and we find a pair of solutions: one positive and
 218 one negative. The negative root is irrelevant, so the remaining solution gives an analytical expression for a
 219 as a function of several parameters and A^* (see S4). Together, these expressions for a and b describe a Hopf
 220 bifurcation manifold that determines whether the nontrivial steady state is stable or whether there is a stable
 221 periodic orbit around it (Figure 4).

222 2.3 Comparison between biological regimes

Regime	Trivial steady state (N^*, A^*, E^*)	Stability Condition	Nontrivial steady state (N^*, A^*, E^*)	Stability Condition	Hopf Bifurcation
Regime 1	$(\frac{a}{b}, 0, 0)$	$\frac{a}{b} < \frac{1}{f-1}, (f > 1)$	$\left(\frac{1}{f-1}, \frac{f(af-a-b)}{e^E_0 c(f-1)}, W\left(d\frac{f(af-a-b)}{c(f-1)}\right)\right)$	$\frac{a}{b} > \frac{1}{f-1}, (f > 1)$	N/A
Regime 2	$(\frac{a}{b}, 0, 0)$	$\frac{a}{b} < \frac{1}{f-1}, (f > 1)$	$\left(\frac{1}{f-1}, \frac{1}{h} W\left(h\frac{f(af-a-b)}{c(f-1)}\right), hA^*\right)$	$\frac{a}{b} > \frac{1}{f-1}, (f > 1)$	N/A
Regime 3	$(\frac{a}{b}, 0, 0)$	$\frac{a}{b} < \frac{1}{f-1}, (f > 1)$	$\left(\frac{1}{f-1}, \frac{1}{d} W\left(d\frac{f(af-a-b)}{c(f-1)}\right), dA^*\right)$	Figure 4	Figure 4

Table 2: Summary comparing asymptotic model behavior across regimes.

223 Across all three Regimes, the trivial steady state, without persistent algae or EPS, is stable when the ratio of
224 nutrient inflow to nutrient loss is too small (i.e. $\frac{a}{b} < \frac{1}{f-1}$ for $f > 1$) (Table 2). In this case, nutrient inflow
225 a is too low to offset physical and biological losses (captured in b , the nutrient loss rate, and f , the algal
226 nutrient uptake rate), preventing algal establishment and resulting in EPS production. Conversely, when
227 nutrient inputs are sufficiently high relative to loss $\left(\frac{a}{b} > \frac{1}{f-1}\right)$, algae persist, with resulting sustained EPS
228 production.

229 The parameters h and d seen in the nontrivial steady state in Regimes 2 and 3 (Table 2) share the same
230 units, and both represent the growth rate of EPS. In Regime 2, the parameter σ represents the efficiency
231 with which algal biomass is converted into EPS, setting the proportionality between algal growth and EPS
232 accumulation. Larger values of σ correspond to more rapid EPS production per unit of algal biomass, while
233 smaller values indicate weaker coupling between algal growth and EPS synthesis. When σ is set to $\sigma = \frac{\rho}{\eta}$,
234 where ρ is the production rate of EPS and η is the degradation of EPS, then $d = h$, leading to identical
235 steady-state behavior in Regimes 2 and 3. In both of these regimes, EPS biomass is directly proportional to
236 algal biomass at steady state.

237 Based on the parameters found in the literature [9, 15], we have $E^* = dA^* > A^*$, indicating that $d, h > 1$.
238 Therefore, in both Regimes 2 and 3, the nontrivial equilibrium EPS concentration exceeds the corresponding
239 algal biomass, consistent with observational studies

To compare the nontrivial algal steady states across the different regimes in Table 2, we begin with the expression

$$x = \frac{f(af - a - b)}{c(f - 1)} > 0,$$

240 which appears in each regime's nontrivial steady state A^* . First, we compare the value of Regime 1, xe^{-E_0} ,
241 to that of Regime 2, $\frac{1}{h}W(hx)$. To determine which is larger, we first find when $\frac{1}{h}W(hx) = xe^{-E_0}$. Let
242 $y = W(hx)$, then

$$\begin{aligned} y &= W(dh) \\ \implies dh &= ye^y \\ hx &= ye^{E_0} \\ ye^y &= ye^{E_0} \\ e^y &= e^{E_0}hx = E_0e^{E_0} \\ x &= \frac{E_0e^{E_0}}{h} \end{aligned}$$

243 When $0 < x < \frac{E_0e^{E_0}}{d}$, the nontrivial steady-state algal biomass in Regime 2 exceeds that in Regime 1, i.e.,
244 $A_2^* > A_1^*$. At the threshold value $x = \frac{E_0e^{E_0}}{d}$, the two regimes yield identical steady-state algal biomass,

245 so that $A_1^* = A_2^*$. For $x > \frac{E_0 e^{E_0}}{d}$, the ordering reverses, and Regime 1 supports a larger asymptotic algal
 246 biomass than Regime 2, i.e., $A_1^* > A_2^*$. An identical comparison holds for Regime 3, as its expression for
 247 A^* differs from that of Regime 2 only by replacing h with d , leading to the same conclusions regarding
 248 the relative magnitudes of the nontrivial steady states. Finally, if $E_0 > 0$, the quantity $\frac{x}{e^{E_0}} < x$ indicates
 249 that regime 1 yields less asymptotic algal biomass than the unmodified baseline value x ; in this case, EPS
 250 reduces the nontrivial steady state algal concentration A^*

251 In summary, the comparison across regimes reveals a clear hierarchy governed by a threshold $x = \frac{E_0 e^{E_0}}{d}$:
 252 Below this threshold, Regimes 2 and 3 support higher asymptotic algal biomass than Regime 1, while above
 253 it, the ordering reverses. Regime 2 serves as an intermediate case, aligning with Regime 3 when $d = h$ and
 254 shifting otherwise. In all cases, EPS reduces steady-state algal biomass relative to the baseline value x , with
 255 the magnitude of this reduction depending on EPS production parameters.

256 2.4 Transient bloom dynamics

257 In addition to studying the asymptotic behavior of algae and EPS, we are also interested in their transient
 258 dynamics during an algal bloom. Transient dynamics occur over shorter, often ecologically important time
 259 scales. Our transient analysis is inspired by that of Huppert (2002), who explored transient bloom dynamics
 260 for a classic model of nutrient-driven phytoplankton blooms [11]. The relative simplicity of that model
 261 allowed for an analytic analysis of the transient dynamics [11]. Adding EPS to the nutrient-algae system
 262 precludes the use of those analytic approaches, so we instead numerically investigate the dependence of the
 263 bloom dynamics on initial conditions, nutrient fluxes, and EPS accumulation and decay rates. To quantify
 264 these effects, we conducted a local sensitivity analysis to determine the parametric dependencies of the
 265 maximum nutrient, algal, and EPS concentrations (N_{max} , A_{max} , and E_{max}) during the algal bloom. We
 266 focus our transient analysis on the model under Regime 3, which makes no strong assumptions about the
 267 timescale of EPS dynamics.

268 Note that we define a “bloom” as occurring whenever there is an initial increase in algae immediately
 269 following time $t = 0$. Mathematically, this requires $\frac{dA}{dt}|_{t=0} > 0$, which necessitates $N_0 > \frac{1}{f-1}$ in (3). In
 270 what follows, we assume N_0 is above this threshold, resulting in an initial increase in $A(t)$. We then vary
 271 parameters by 50-150% in the dimensional model (2) around the values in Table 1.

272 **Influence of nutrient fluxes on bloom peaks** Previous work on nutrient-driven phytoplankton dynamics
 273 suggests that an increase in the nutrient inflow rate leads to higher phytoplankton and nutrient peaks [11],
 274 and vice versa for the nutrient loss rate. Consistent with these findings, we observe that increasing ϕ results
 275 in higher maximum concentrations of algae (A_{max}), nutrients (N_{max}), and EPS (E_{max}), while increasing
 276 ψ lowers them (Figure 5).

277 **Influence of algal growth and loss rates on bloom peaks** As the nutrient uptake rate of bottom-ice
 278 algae, ν , increases, N_{max} decreases, while A_{max} and E_{max} both increase, as one may have intuitively
 279 expected (Figure 5). Similarly, decreasing the nitrogen half-saturation constant, γ , should increase the rate
 280 of nutrient uptake by algae, but within the tested range γ has little effect on bloom peaks (Figure 5). In
 281 contrast, increasing the algal mortality rate, δ , produces the expected effect: both A_{max} and E_{max} decline,
 282 while N_{max} remains largely unchanged (Figure 5). Finally, increasing the chl a to nitrogen conversion ratio,
 283 ξ , increases both algal and EPS peaks, accompanied by a slight reduction in the nutrient maximum (Figure
 284 5).

285 **Influence of EPS accumulation and loss rates on bloom peaks** EPS influences bloom dynamics in ways
 286 consistent with the hypothesized EPS-mediated feedback mechanism. Increasing the EPS production rate ρ
 287 leads to a higher maximum EPS concentration (E_{max}), while reducing the peak of the algal bloom (A_{max})
 288 (Figure: 5). Similarly, increasing the degradation rate of EPS η causes E_{max} to decrease while N_{max} and
 289 A_{max} to increase (Figure 5). These inverse relationships between peak EPS accumulation and peak bloom
 290 intensity suggest that the negative EPS-mediated biophysical feedback, which is the focus of this paper,
 291 reduces peak algal concentrations, in addition to the reduction in asymptotic algal concentrations explored
 292 earlier.

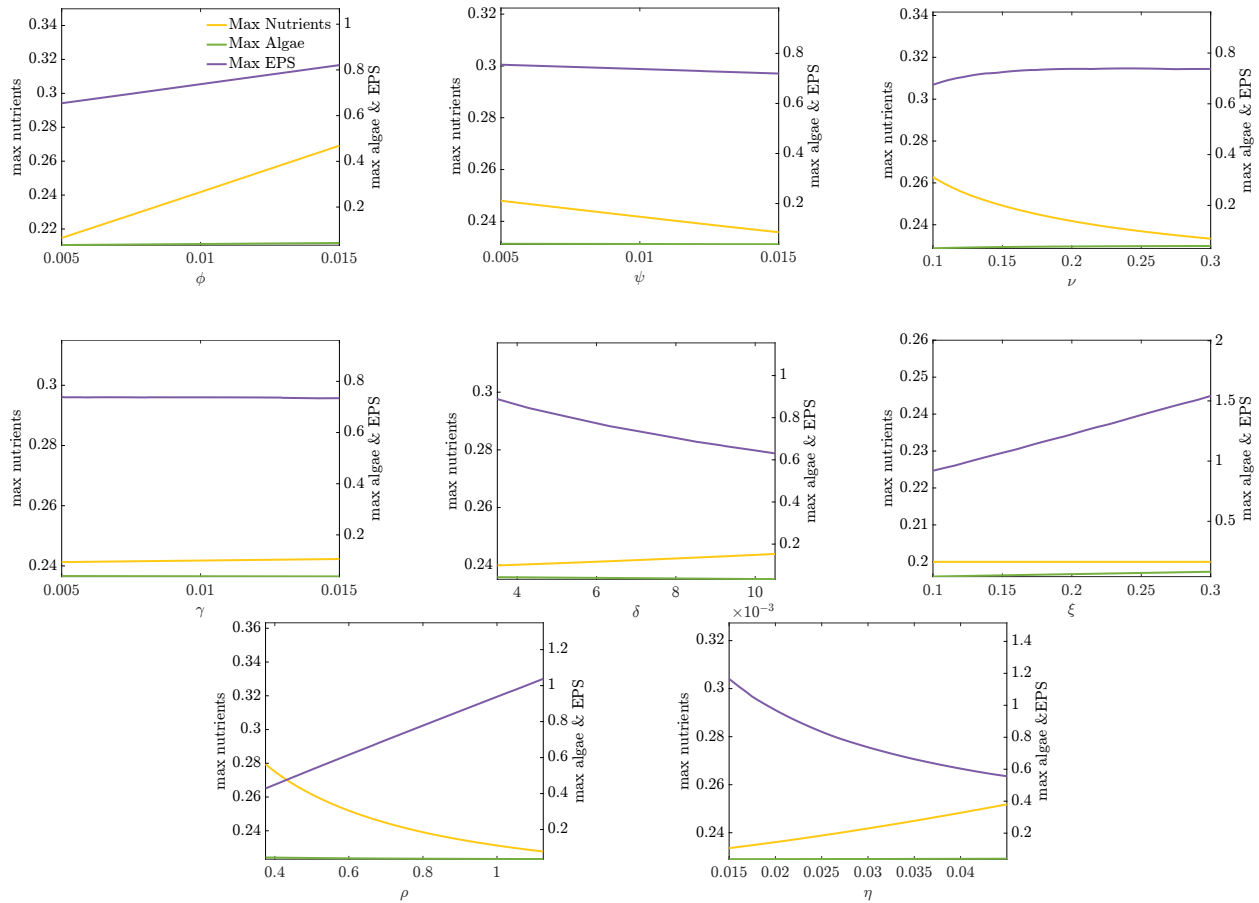


Figure 5: Each graph represents the effects that each parameter has on the nutrient, algal, and EPS concentration peaks (N_{max} , A_{max} , E_{max} respectively). Parameter values were chosen to be between 50% and 150% of the values in Table 1.

293 3 Real world model implications

294 We selected parameter values consistent with observations in polar sea ice systems (Table 1). These val-
 295 ues include both empirically measured quantities and reasonable estimates derived from biogeochemical
 296 literature, and are intended to capture a range of plausible conditions encountered within sea ice.

297 Figure 6 shows the solution of model 2 using the parameter values in Table 1. Here we see that high nutrient
 298 concentrations initially support rapid algal growth and subsequent EPS production. Eventually, as nutrients
 299 are depleted, the bloom ends and the system transitions to a nutrient-limited state [14, 2].

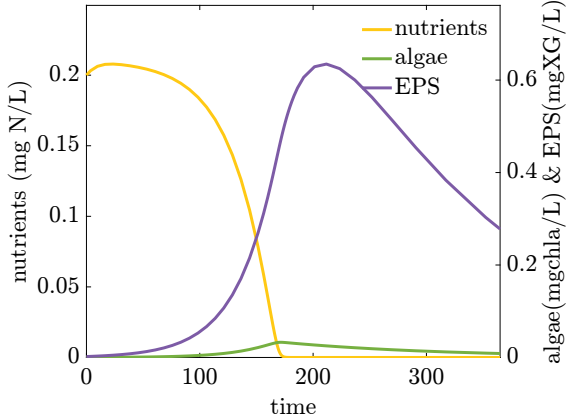


Figure 6: Time series of nutrients, algae, and EPS over the first simulated year. Algal biomass and EPS persist while nutrient concentrations are gradually depleted to a sustained level, consistent with observations found from Arctic sea ice ecosystems. The modeled concentrations of nutrients, algae, and EPS during a bloom fall within reported ranges in the literature, indicating a realistic parameterization. However, the duration of the simulated algal bloom happens later than typically observed in field studies. Parameter values are as in Table 1

300 4 Discussion

301 In this paper, we extended a classic nutrient-algae model to include EPS-mediated biophysical feedbacks.
 302 We considered three regimes to distinguish between possible timescales of EPS dynamics. All regimes share
 303 two asymptotic scenarios: one in which EPS, algae, and nutrients persist, and another in which, despite sus-
 304 tained nutrient availability, algae and EPS do not persist. Notably, the shift between these two asymptotic
 305 states depends only on a combination of the nutrient fluxes and the growth rate of algae; the bifurcation
 306 is unrelated to EPS dynamics, and is consistent with the bifurcation found in the nutrient-phytoplankton
 307 model, without EPS [11]. In all regimes, reductions in permeability caused by EPS accumulation lead to
 308 lower asymptotic nutrient availability, ultimately suppressing algal growth and altering system stability.
 309 When the feedback is sufficiently strong, this results in periodic solutions, highlighting the role of EPS in
 310 determining whether the system approaches a steady state or oscillatory behavior. Thus, across regimes,
 311 the system's qualitative behavior remains consistent, even as the quantitative solutions differ slightly. This
 312 robustness suggests that the essential feedback mechanics governing EPS and algal interactions are pre-
 313 served regardless of the timescale assumptions on EPS. Analysis of model transient dynamics revealed that
 314 EPS-mediated biophysical feedbacks also reduce bloom intensity, suggesting that these feedbacks have both
 315 short and long-term implications for primary productivity within the ice.

316 Perhaps the most salient unknown in our models is which functional form best describes the effects of EPS
 317 on nutrient fluxes. In addition to the exponential form analyzed here, we also considered an alternate, Hill
 318 function for the nutrient flux terms ($\alpha(E)$ and $\beta(E)$) (Appendix A). This analysis demonstrates that varying
 319 the feedback strength encoded by the Hill function can qualitatively alter the system's dynamics, including
 320 the emergence of a Hopf bifurcation that is absent under weaker feedback. Future empirical and modeling
 321 studies are needed to improve our confidence in the functional forms for $\alpha(E)$ and $\beta(E)$.

322 While our asymptotic analyses suggest EPS suppresses asymptotic algal concentrations and may even cause
 323 periodic solutions, real sea ice ecosystems are governed by significant additional complexities such as sea-

324 sonal temperature fluctuations. These temperature swings shape ice and snow dynamics, which determine
325 the amount of light available for photosynthesis within the ice and the availability and stability of the ice
326 substrate as an algal habitat [21]. Additional biological interactions, including those with heterotrophic
327 grazers and viral interactions, as well as competition with other organisms for light and nutrients, introduce
328 further complexity not considered here. Future modeling efforts could merge models of these more complex
329 dynamics with the EPS-mediated feedbacks explored here.

330 This modeling study represents a novel approach to integrating dynamic sea-ice biology and physics at the
331 microscale. Previous studies have treated these processes independently, focusing on either sea ice biogeo-
332 chemistry or physics within sea ice [17, 19, 22, 26]. This study is, to the best of our knowledge, the first
333 to quantitatively investigate the influence of EPS on sea ice permeability and the resulting impacts on algal
334 growth. The EPS-mediated feedbacks explored here suppressed algal biomass both during the bloom and
335 asymptotically, while simultaneously reducing ice permeability, highlighting the tight coupling between sea
336 ice permeability and biological productivity.

337 **5 Author contribution**

338 ARJ led all aspects of the study, including model development, analysis, and manuscript preparation. JRR
339 contributed substantially to the study's conceptualization and to the initial manuscript draft. All other au-
340 thors contributed to manuscript editing and revisions.

341 **6 Acknowledgments**

342 **7 Supporting information**

343 All supplemental information, analysis, and code used to generate all figures are available in a Github
344 repository. A corresponding DOI will be created following acceptance for publication.

345 **Appendix A: Hill functional form**

346 Based on our findings above that EPS-mediated feedback can result in periodic solutions, we now ask what
 347 level of negative feedback is required for the system to exhibit this periodic behavior. To explore the impacts
 348 of an alternative functional choice for the nutrient flux terms, we introduce an alternative functional form for
 349 $\alpha(E)$ and $\beta(E)$. The Hill function captures saturation effects by modeling how increasing EPS diminishes
 350 feedback strength on nutrient inflow and outflow. This reflects some intuition that, beyond a certain concen-
 351 tration, additional EPS may have little additional impact on nutrient dynamics. We set $\alpha(E) = \frac{\phi}{(1+\mu E)^p}$ and
 352 $\beta(E) = \frac{\psi}{(1+\mu E)^p}$ in (1), where p controls the level of negative feedback. Nondimensionalization yields

$$\epsilon \frac{dN}{dt} = \frac{a}{(1+E)^p} - \frac{cNA}{1+N} - \frac{bN}{(1+E)^p} \quad (13a)$$

$$\epsilon \frac{dA}{dt} = \frac{fNA}{1+N} - A \quad (13b)$$

$$\frac{dE}{dt} = dA - E \quad (13c)$$

353 Note that the system is nondimensionalized with the same parameters as before (see S6) to aid in interpre-
 354 tation. This system, like the previous ones, has a trivial and nontrivial equilibrium,

$$g_0 = \left(\frac{a}{b}, 0, 0 \right)$$

$$g_1 = \left(\frac{1}{f-1}, \frac{\left(\frac{c}{f-1} - a \right) \left(1 + \frac{1}{f-1} \right)}{(E+1)^p \left(\frac{c}{f-1} \right)}, Ad \right)$$

We evaluate the Jacobian of (13) at g_0 and find the eigenvalues:

$$\mu_1 = -1, \mu_2 = -b, \mu_3 = \frac{fa - a - b}{b + a}.$$

355 As before, the stability of the trivial solution g_0 is lost when $\frac{a}{b} > \frac{1}{f-1}$. The remaining stability analysis
 356 continues to follow the analysis of Section 2.2.3 (see S6). We highlight here how the results of model (13)
 357 differ from those of model (2), which had exponential terms for $\alpha(E)$ and $\beta(E)$. In this model, we can vary
 358 p , the strength of the EPS-mediated feedback in the system, and as we do so, a Hopf bifurcation emerges
 359 (Figure A1), suggesting that a stronger feedback induces periodic behavior. Exploring this relationship
 360 further, we see that a higher nutrient inflow promotes oscillations, but only if the negative feedback is not
 361 too strong. As feedback strength increases, less nutrient inflow is needed to induce a Hopf bifurcation. This
 362 result suggests that EPS can destabilize or stabilize the system depending on how strongly EPS feeds back
 363 on nutrient dynamics (Figure A1).

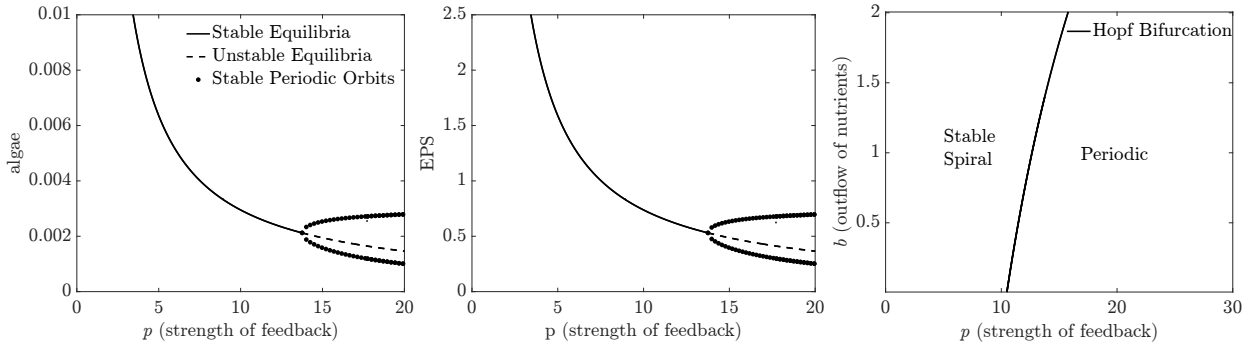


Figure A1: **Left:** Algal bifurcation diagram of feedback strength p showing that as p increases a periodic solution appears. **Middle:** EPS bifurcation diagram of feedback strength p showing that as p increases a periodic solution appears. **Right:** Two-parameter bifurcation graph. On one side of the curve, there is a stable spiral towards the equilibrium point g_1 , while on the other side, there is a periodic orbit around g_1 . All parameter values are as in Table 1.

364 Appendix B: Regime 2 trace is always negative

365 We show here that the trace $Tr(J_{r_1})$ in (12) is negative by proof by contradiction. Assume both $b > 0$ and
 366 $Tr(J_{r_1}) > 0$. Then it follows from (10) that $\text{sign}(b) = \text{sign}(afe^{-hA^*} - cA^*)$ and the
 367 $\text{sign}(Tr(J_{r_1})) = \text{sign}(-e^{-hA^*}af^2 + cA^*)$ from equation (12). Using the fact that $b > 0$ and $Tr(J_{r_1}) > 0$
 368 gives:

$$\begin{aligned} afe^{-hA^*} &> cA^* > af^2e^{-hA^*} \\ \implies f &> \frac{cA^*}{ae^{-hA^*}} > f^2 \end{aligned}$$

369 However, assuming that $f > 1$ implies that $f^2 > f$, contradicting the inequality $f > f^2$. Thus, there is
 370 no regime where both $Tr(J_{r_1}) > 0$ and $b > 0$. Thus, $Tr(J_{r_1}) > 0 \implies b < 0$, which lies outside the
 371 biologically meaningful parameter regime.

372 Appendix C: Nondimensional parameters for regime 1 and 3

$$\begin{aligned} N^* &= \frac{N}{\gamma} & a &= \frac{\phi}{\gamma\delta} \\ A^* &= \frac{A}{\gamma} & b &= \frac{\psi}{\delta} \\ E^* &= \frac{E}{\mu} & c &= \frac{\nu}{\delta} \\ t &= \frac{\tau}{\eta} & d &= \frac{\rho\gamma}{\mu\eta} \\ f &= \xi c & \epsilon &= \frac{\eta}{\delta} \end{aligned}$$

³⁷³ **Appendix D: Nondimensional parameters for regime 2**

$$\begin{aligned} N^* &= \frac{N}{\gamma} & a &= \frac{\phi}{\gamma\delta} \\ A^* &= \frac{A}{\gamma} & b &= \frac{\psi}{\delta} \\ t &= \frac{\tau}{\delta} & c &= \frac{\nu}{\delta} \\ f &= \xi c & h &= \frac{\sigma\gamma}{\mu} \end{aligned}$$

374 **References**

375 [1] Kevin R. Arrigo, Gert Van Dijken, and Sudeshna Pabi. “Impact of a shrinking Arctic ice cover on ma-
376 rine primary production”. en. In: *Geophysical Research Letters* 35.19 (Oct. 2008), 2008GL035028.
377 ISSN: 0094-8276, 1944-8007. DOI: 10.1029/2008GL035028. URL: <https://agupubs.onlinelibrary.wiley.com/doi/10.1029/2008GL035028> (visited on 03/03/2025).

378 [2] R. Eric Collins, Shelly D. Carpenter, and Jody W. Deming. “Spatial heterogeneity and temporal
379 dynamics of particles, bacteria, and pEPS in Arctic winter sea ice”. en. In: *Journal of Marine Systems*
380 74.3-4 (Dec. 2008), pp. 902–917. ISSN: 09247963. DOI: 10.1016/j.jmarsys.2007.09.005.

381 [3] G.S Dieckmann D.N Thomas. “Sea Ice”. In: 2 (2010), pp. 247–275. ISSN: 9781444317145. DOI:
382 10.1002/9781444317145.

383 [4] Alan Decho. “Decho AW.. Microbial exopolymer secretions in ocean environments: their role(s) in
384 food webs and marine processes. *Oceanogr Mar Biol Ann Rev* 28: 73-153”. In: *Oceanography and*
385 *marine biology annual review* 28 (Jan. 1990), pp. 73–154.

386 [5] Marcela Ewert and Jody Deming. “Sea Ice Microorganisms: Environmental Constraints and Extracel-
387 lular Responses”. en. In: *Biology* 2.2 (Mar. 2013), pp. 603–628. ISSN: 2079-7737. DOI: 10.3390/
388 *biology*20200603.

389 [6] François Fripiat et al. “High turnover rates indicated by changes in the fixed N forms and their stable
390 isotopes in Antarctic landfast sea ice”. In: *Journal of Geophysical Research: Oceans* 120.4 (2015),
391 pp. 3079–3097.

392 [7] R Gradinger and J Ikävalko. “Organism incorporation into newly forming Arctic sea ice in the Green-
393 land Sea”. In: *Journal of plankton research* 20.5 (1998), pp. 871–886.

394 [8] Rolf Gradinger. “Sea-ice algae: Major contributors to primary production and algal biomass in the
395 Chukchi and Beaufort Seas during May/June 2002”. en. In: *Deep Sea Research Part II: Topical*
396 *Studies in Oceanography* 56.17 (Aug. 2009), pp. 1201–1212. ISSN: 09670645. DOI: 10.1016/j.
397 *dsr2.2008.10.016*. URL: <https://linkinghub.elsevier.com/retrieve/pii/S0967064508003469> (visited on 03/03/2025).

398 [9] Elizabeth Hunke et al. *CICE-Consortium/Icepack: Icepack 1.5.0*. Nov. 2024. DOI: 10.5281/
399 zenodo.14188409. URL: <https://doi.org/10.5281/zenodo.14188409>.

400 [10] Elizabeth C. Hunke, William H. Lipscomb, and Adrian K. Turner. “Sea-ice models for climate study:
401 retrospective and new directions”. en. In: *Journal of Glaciology* 56.200 (2010), pp. 1162–1172. ISSN:
402 0022-1430, 1727-5652. DOI: 10.3189/002214311796406095.

403 [11] Amit Huppert, Bernd Blasius, and Lewi Stone. “A Model of Phytoplankton Blooms”. en. In: *The*
404 *American Naturalist* 159.2 (Feb. 2002), pp. 156–171. ISSN: 0003-0147, 1537-5323. DOI: 10.1086/
405 324789.

406 [12] Kwanwoo Kim et al. “Carbon and nitrogen uptake rates and macromolecular compositions of bottom-
407 ice algae and phytoplankton at Cambridge Bay in Dease Strait, Canada”. en. In: *Annals of Glaciology*
408 61.82 (Sept. 2020), pp. 106–116. ISSN: 0260-3055, 1727-5644. DOI: 10.1017/aog.2020.17.
409 URL: https://www.cambridge.org/core/product/identifier/S0260305520000178/type/journal_article (visited on 04/07/2025).

410 [13] Klaudia Kosek et al. “Phytoplankton communities of polar regions Diversity depending on environ-
411 mental conditions and chemical anthropopressure”. en. In: *Journal of Environmental Management*
412 171 (Apr. 2016), pp. 243–259. ISSN: 03014797. DOI: 10.1016/j.jenvman.2016.01.026.

413

414

415

416 [14] C Krembs et al. "High concentrations of exopolymeric substances in Arctic winter sea ice: impli-
417 cations for the polar ocean carbon cycle and cryoprotection of diatoms". en. In: *Deep Sea Research*
418 *Part I: Oceanographic Research Papers* 49.12 (Dec. 2002), pp. 2163–2181. ISSN: 09670637. DOI:
419 10.1016/S0967-0637(02)00122-X.

420 [15] Christopher Krembs, Hajo Eicken, and Jody W. Deming. "Exopolymer alteration of physical proper-
421 ties of sea ice and implications for ice habitability and biogeochemistry in a warmer Arctic". en. In:
422 *Proceedings of the National Academy of Sciences* 108.9 (Mar. 2011), pp. 3653–3658. ISSN: 0027-
423 8424, 1091-6490. DOI: 10.1073/pnas.1100701108.

424 [16] R. A. Lake and E. L. Lewis. "Salt rejection by sea ice during growth". en. In: *Journal of Geophysical*
425 *Research* 75.3 (Jan. 1970), pp. 583–597. ISSN: 01480227. DOI: 10.1029/JC075i003p00583.
426 URL: <http://doi.wiley.com/10.1029/JC075i003p00583> (visited on 03/03/2025).

427 [17] Delphine Lannuzel et al. "The future of Arctic sea-ice biogeochemistry and ice-associated ecosys-
428 tems". en. In: *Nature Climate Change* 10.11 (Nov. 2020), pp. 983–992. ISSN: 1758-678X, 1758-6798.
429 DOI: 10.1038/s41558-020-00940-4.

430 [18] K Meiners et al. "Vertical distribution of exopolymer particles in sea ice of the Fram Strait (Arctic)
431 during autumn". en. In: *Marine Ecology Progress Series* 248 (2003), pp. 1–13. ISSN: 0171-8630,
432 1616-1599. DOI: 10.3354/meps248001.

433 [19] Lisa A. Miller et al. "Methods for biogeochemical studies of sea ice: The state of the art, caveats,
434 and recommendations". en. In: *Elementa: Science of the Anthropocene* 3 (Jan. 2015). Ed. by Jody
435 W. Deming and Stephen F. Ackley, p. 000038. ISSN: 2325-1026. DOI: 10.12952/journal.
436 elementa.000038.

437 [20] Chris Petrich and Hajo Eicken. "Growth, Structure and Properties of Sea Ice". In: *Sea Ice*. John
438 Wiley Sons, Ltd, 2009. Chap. 2, pp. 23–77. ISBN: 9781444317145. DOI: <https://doi.org/10.1002/9781444317145.ch2>. eprint: <https://onlinelibrary.wiley.com/doi/pdf/10.1002/9781444317145.ch2>. URL: <https://onlinelibrary.wiley.com/doi/abs/10.1002/9781444317145.ch2>.

442 [21] A Riedel, C Michel, and M Gosselin. "Seasonal study of sea-ice exopolymeric substances on the
443 Mackenzie shelf: implications for transport of sea-ice bacteria and algae". en. In: *Aquatic Microbial*
444 *Ecology* 45 (Nov. 2006), pp. 195–206. ISSN: 0948-3055, 1616-1564. DOI: 10.3354/ame045195.

445 [22] Arnout Roukaerts et al. "The biogeochemical role of a microbial biofilm in sea ice". en. In: *Elem Sci*
446 *Anth* 9.1 (June 2021), p. 00134. ISSN: 2325-1026. DOI: 10.1525/elementa.2020.00134.

447 [23] Jennifer Routledge et al. "Unprecedented shift in Canadian High Arctic polar bear food web unsettles
448 four millennia of stability". en. In: *Anthropocene* 43 (Sept. 2023), p. 100397. ISSN: 22133054. DOI:
449 10.1016/j.ancene.2023.100397. URL: <https://linkinghub.elsevier.com/retrieve/pii/S2213305423000309> (visited on 03/03/2025).

451 [24] Kyle R. Steffen et al. "Network Modeling of Fluid Transport Through Sea Ice with Entrained Ex-
452 opolymeric Substances". en. In: *Multiscale Modeling & Simulation* 16.1 (Jan. 2018), pp. 106–124.
453 ISSN: 1540-3459, 1540-3467. DOI: 10.1137/17M1117513.

454 [25] Dk Stoecker et al. "Primary production in the upper sea ice". en. In: *Aquatic Microbial Ecology* 21
455 (2000), pp. 275–287. ISSN: 0948-3055, 1616-1564. DOI: 10.3354/ame021275. URL: <http://www.int-res.com/abstracts/ame/v21/n3/p275-287/> (visited on 03/03/2025).

457 [26] Letizia Tedesco and Marcello Vichi. "Sea Ice Biogeochemistry: A Guide for Modellers". en. In:
458 *PLoS ONE* 9.2 (Feb. 2014). Ed. by João Miguel Dias, e89217. ISSN: 1932-6203. DOI: 10.1371/journal.pone.0089217.

460 [27] David N. Thomas and G. S. Dieckmann. *Sea Ice: an Introduction to its Physics, Chemistry, Biology*
461 and Geology. en. OCLC: 437218678. Chichester: John Wiley & Sons, 2008. ISBN: 978-0-470-75692-
462 8.

463 [28] Rui Xiao and Yi Zheng. “Overview of microalgal extracellular polymeric substances (EPS) and their
464 applications”. en. In: *Biotechnology Advances* 34.7 (Nov. 2016), pp. 1225–1244. ISSN: 07349750.
465 DOI: 10.1016/j.biotechadv.2016.08.004.

466 [29] J. Zhu et al. “A network model for fluid transport through sea ice”. en. In: *Annals of Glaciology*
467 44 (2006), pp. 129–133. ISSN: 0260-3055, 1727-5644. DOI: 10.3189/172756406781811141.
468 URL: https://www.cambridge.org/core/product/identifier/S0260305500254797/type/journal_article (visited on 08/07/2024).

470 [30] Z. Zong. “A Random Pore Model of sea ice for predicting its mechanical properties”. en. In: *Cold*
471 *Regions Science and Technology* 195 (Mar. 2022), p. 103473. ISSN: 0165232X. DOI: 10.1016/
472 j.coldregions.2021.103473. URL: <https://linkinghub.elsevier.com/retrieve/pii/S0165232X21002548> (visited on 03/03/2025).

473